Emmanuel Rieborue Khama[1], Emmanuel Zeneboebi Loyibo[2], Wilfred Okologume[2], Stanley Toochukwu Ekwueme[3], Chukwudi Victor Okafor[2], Nnaemeka Princewill Ohia[3]*

[1]Nigeria Maritime University, Okerenkoko, Delta State, Nigeria, [2]Department of Petroleum Engineering, Federal University of Petroleum Resources, Effurun, Nigeria, [3]Department of Petroleum Engineering, Federal university of Technology, Owerri, Nigeria

Scientific paper
ISSN 0351-9465, E-ISSN 2466-2585
https://doi.org/10.62638/ZasMat1149

Zastita Materijala 65 (2)
258 - 272 (2024)

Investigation of the performance of activated carbon derived from ripe plantain peels for CO_2 capture: Modelling and optimisation using response surface methodology

ABSTRACT

This study investigates the potential of activated carbon derived from ripe plantain peels (PPAC) for carbon dioxide (CO_2) capture. PPAC was prepared through carbonization and activation using H_3PO_4, and its unique properties were extensively characterized which revealed irregular sponge-like protrusions and well-defined pores under Scanning Electron Microscopy (SEM). Elemental analysis identified carbon, silicon, and oxygen as major components, corroborated by X-ray Diffraction (XRD) analysis indicating the presence of silicon oxide (SiO_2), potassium oxide (K_2O), and calcium oxide (CaO). Fourier Transform Infrared (FTIR) spectroscopy highlighted diverse functional groups on PPAC's surface. CO_2 adsorption tests were conducted at 27°C and 40°C with varying pressures on PPAC particles of 150µm and 845µm sizes. Results revealed that CO_2 adsorption capacity increased with escalating pressures. Remarkably, at 27°C, PPAC exhibited superior performance than at 40°C, attributed to a higher-pressure drop enhancing the driving force for CO_2 adsorption. Larger particles (845µm) demonstrated higher adsorption capacity due to increased surface area, enhanced pore accessibility, and faster mass transfer. The Response Surface Methodology (RSM) conducted gave 2FI model as the most representative of the design data and showed high accuracy (R^2=0.9973) and low error metrics (MSE=0.01697, RMSE=0.130269, MAE=0.109, MAPE=2.7244). The Adeq Precision value of 76.26 validated the model's reliability. Optimization using RSM yielded optimal CO_2 adsorption values (9.69 mmol/g) at 27°C and 100 bars. PPAC emerges as a promising solution for CO_2 capture, offering valuable prospects in mitigating emissions and addressing climate change challenges.

***Keywords**: Ripe Plantain peel activated carbon, Response surface methodology, Characterization, optimisation, CO_2 adsorption*

1. INTRODUCTION

The utilization of fossil fuels has resulted in substantial CO_2 emissions, a major contributor to global warming and climate change [1,2]. CO_2 emissions constitute a significant portion of global greenhouse gas emissions, posing challenges such as climate change and ocean acidification [3, 4]. Currently, atmospheric CO_2 levels have exceeded 415 ppm, surpassing the Earth's capacity. Rising global temperatures, particularly beyond 2℃, could lead to severe environmental consequences [5,6].

Efforts to mitigate global warming include the exploration of Carbon Capture and Storage (CCS) technologies. Among these, post-combustion CO_2 capture techniques, have gained prominence due to their low technological risk and retrofittable nature [7,8]. Various methods, such as adsorption, membrane processes, cryogenic distillation, and adsorption, have been suggested for CO_2 separation [6, 9]. Among these options, cryogenic distillation is the most established, but its extensive use is hindered by significant energy consumption and high costs [10,11].

Absorption methods, especially those utilizing amine-based solvents, offer high CO_2 absorption rates but are hindered by high costs, energy consumption, corrosion issues, and environmental concerns [11,12]. Additionally, liquid sorbents like polyamines and organic-inorganic hybrids necessitate thermal energy for desorption [13,14].

*Corresponding author: Stanley Toochukwu Ekwueme
E-mail: stanleyekwueme@yahoo.com
Paper received: 17. 11. 2023.
Paper accepted: 10. 12. 2023.
Paper is available on the website: www.idk.org.rs/journal

Membrane separation, on the other hand, has emerged as a promising technology for CO_2 capture. Both polymeric and inorganic membranes have been extensively studied [15,16]. Inorganic membranes have demonstrated high permeability and selectivity but face challenges related to fabrication costs and scalability [17,18]. Polymeric membranes, following the solution-diffusion mechanism, encounter limitations due to the trade-off between selectivity and permeability, hindering their industrial applicability [19,20].

Adsorption-based CO_2 capture, employing materials like activated carbon (AC), metal-organic frameworks (MOFs), zeolite molecular sieves, and porous organic polymers (POPs), has gained attention, especially for smaller-scale applications [17, 20]. Among these, AC stands out due to its low regeneration energy, thermal stability, large porosity, and cost-effectiveness. While commercially-produced AC exhibits good performance, its production process is prohibitively expensive in developing nations, leading to increased operational costs [21,22].

To address these challenges, there is a growing interest in affordable methods of producing activated carbon. Utilizing biomass from agricultural waste materials such as rice husk, coconut husk, plantain peels, sawdust, bagasse, and other agricultural residues presents an economical and environmentally sustainable alternative [23,24]. These biomass-derived sources significantly reduce production costs compared to commercial counterparts and hold great potential for future commercialization [25-27].

Researchers have extensively explored the utilization of biomass and waste materials for the preparation of activated carbon with promising applications in CO_2 adsorption [28,29]. For instance, Sabri et al. [30] investigated the use of palm kernel shell for activated carbon synthesis, which was further modified with imidazoles. This modified activated carbon demonstrated outstanding performance in CO_2 capture during pressure swing adsorption processes [31,32].

Serafin et al. [20] explored the use of Amazonian andiroba shell for producing porous activated carbon as a CO_2 adsorbent. They employed physical activation techniques and studied the effect of activation times on the material's characteristics. The resulting activated carbon exhibited high surface area, microporosity, and excellent CO_2 adsorption capacity. Additionally, their research highlighted the material's superior cyclic stability and charge transfer processes, indicating its potential for practical applications.

Patel et al. [19] investigated activated porous carbon derived from pine sawdust using a hybrid synthesis protocol. This research compared the effectiveness of activated carbon derived via physicochemical, chemical, and physical activation methods. The optimized material exhibited a high BET surface area and remarkable CO_2 adsorption capacity. It displayed strong physisorption behaviour for CO_2, making it suitable for repeated adsorption-desorption cycles.

Yanti et al. [21] explored the synthesis of activated carbon from banana peel, which was further modified with magnetite for enhanced iron metal ion recovery. The activated carbon exhibited improved thermal stability after alkali activation. Their study showcased the material's potential in CO_2 adsorption and highlighted its thermal stability after modification.

In recent years, Response Surface Methodology (RSM) has gained widespread popularity for exploring the intricate relationships between responses and independent variables in various chemical processes. RSM has been recognised for its ability to comprehensively consider interactions among variables, both in combination and independently [6]. Unlike the conventional method of altering one variable at a time (OVAT), which is time-consuming, costly, and fails to capture interactions between input variables, RSM modelling and optimization provide a more efficient approach. To facilitate RSM studies, several design techniques are available, such as Box-Behnken Design (BBD), central composite design, and optimal design methods. Among these, the Box-Behnken Design (BBD) has emerged as the most extensively explored method for RSM modelling and optimization. BBD not only reduces the number of experiments required but also offers valuable insights into how processes are influenced by the interactions between various parameters [33].

Many scholars have investigated the use of RSM for modelling and optimisation of activated carbons prepared using biomass precursors. Greco et al. [6] investigated activated carbon prepared from wheat straw using a one-step synthesis approach, comparing it with conventional two-step production methods. Their research demonstrated that the one-step activated carbon exhibited comparable textural properties, CO_2 uptake, and selectivity to the two-step counterparts. Breakthrough curve simulations also emphasized its effectiveness in CH_4/CO_2 separation under dynamic conditions, making the one-step process an economically attractive route for large-scale production systems.

Khoshraftar and Ghaemi [10] investigated the use of pistachio shells for creating microporous activated carbon with high CO_2 adsorption capacity. They employed various analytical techniques such as X-ray diffraction, Fourier transform infrared spectrometry, and scanning electron microscopy to characterize the material. The activated carbon derived from pistachio shells exhibited specific surface area and excellent CO_2 sorption properties. Their study also utilized response surface methodology and artificial neural network models to optimize CO_2 adsorption conditions, achieving highly accurate predictions.

Li et al. [24] explored the synthesis of low-cost activated carbons using apple tree pruning waste and waste polyethylene terephthalate (PET) plastic bottles. Their research focused on understanding the synergistic mechanism between these precursors during carbonization. Through response surface methodology, they analysed the impact of PET ratio and carbonization conditions on pore structure and CO_2 adsorption performance. The optimized conditions led to a significant CO_2 uptake, demonstrating the potential of this activated carbon for CO_2 adsorption.

Mukherjee et al. [30] utilized spent coffee grounds as a feedstock for activated carbon synthesis via physical activation. They optimized the activation parameters using the Box-Behnken design method, achieving high specific surface area. Additionally, they employed a natural deep eutectic solvent to modify the activated carbon's surface functionalities. The resulting material displayed excellent CO_2 capture performance, selectivity, and cyclic stability, making it a promising solution for CO_2 emission mitigation.

2. MATERIALS AND METHODS

2.1. Materials and Apparatus

The study used ripe plantain peel as the precursor material which was obtained from Effurun market in Delta State, Nigeria. H_3PO_4, pure CO_2 gas and distilled water were obtained from the lab. The Apparatus used include SEM device, FTIR device, XRD device, EDX device, grinding machine, stirrer, pH meter, cylindrical glass beaker, oven, furnace, CO_2 adsorption setup.

2.2. Methods

The methods comprise the preparation of plantain peel activated carbon (PPAC), the characterization of the PPAC, the CO_2 adsorption test and the RSM modelling.

2.2.1. Preparation of Activated Carbon

The ripe plantain-peels were thoroughly washed with tap followed by distilled water and sun dried for three weeks. The sun-dried sample was then taken to the lab for extra effective drying using oven at 100^{o}C. The resulting oven-dried sample was taken to the furnace for carbonization. Carbonisation of the oven-dried sample was done at 500^{o}C in the furnace after which the resulting sample was grinded to obtain a smooth powdered sample. The resulting powdered sample was then sieved to several sizes including 150 microns and 840 microns respectively.

Figure 1. PPAC preparation process

Slika 1. Proces pripreme PPAC-a

The resulting sieved carbonized sample was then taken for activation. Phosphoric acid (H_3PO_4) was used as the activator. First, a cylindrical glass beaker was filled with phosphoric acid and then the sieved carbonized sample was added to it. The resulting mixture was vigorously stirred using electric stirrer for 24 hours to achieve a strong cohesion between the activator (H_3PO_4) and the carbonized plantain peel sample. Furthermore, the stirring enabled the H_3PO_4 to achieve strong internal contact with the carbonized material.

The stirring was immediately proceeded with the filtration of the H_3PO_4 acid from the activated sample. Then warm water was added and stirred again to remove residual acid. The pH of the activated carbon was then checked and recorded. The pH was recorded to be 7.60. then the activated carbon was then dried in the oven at 100^{o}C.

2.2.2. Characterisation of the Plantain Peel Activated Carbon

Various characterization techniques were employed to analyze the structural and morphological properties of the plantain peel activated carbon (PPAC). Fourier-Transform Infrared (FTIR) Spectroscopy was used to examine the functional groups in PPAC by analyzing infrared spectra at different wavelengths. A PerkinElmer FTIR spectrometer identified functional groups on PPAC surfaces after mixing PPAC and potassium bromide (KBr) at a weight ratio of 1:200 (g adsorbent/g KBr) and compacting the powder with a hydraulic press to form pellets.

Figure 2. The Activated carbon preparation process (a) ripe plantain peel, (b) carbonized plantain peel, (c) activation of carbonised plantain peel carbon (d) activated plantain peel carbon.

Slika 2. Proces pripreme aktivnog uglja (a) zrela kora banane, (b) karbonizovana kora banane, (c) aktivacija karbonizovanog ugljenika od kore banane (d) aktivni ugljen od kore banana

Scanning Electron Microscopy (SEM) was utilized to observe the morphology of PPAC using a TESCAN Vega 3 model operating at 25 kV. The Micromeritics ASAP 2020 porosimeter measured nitrogen adsorption/desorption isotherms at 77 K to determine the structural parameters of activated carbon. Energy Dispersive X-ray (EDX) analysis was conducted to analyze the chemical composition of the PPAC sample.

The crystalline structure of the sample was determined using X-ray diffraction analysis performed with a D8 Advance X-ray diffractometer (model: D8 Advance, BRUKER, Germany) coupled with a P2 Phaser Bruker and an XFlash silicon drift detector. During the analysis, the sample was ground into a fine powder and placed inside the device. The X-ray motion moved in a circular path from 5 to 90 degrees relative to the horizon line, directing the beam onto the sample from different angles. Diffraction measurements were taken at every 0.015 θ, generating a diffraction pattern.

2.2.3. CO_2 Adsorption Experiment

An experimental setup illustrated in Figure 3a was setup to determine the CO_2 adsorption capacity of PPAC under post-combustion conditions, adhering to Sieverts law [34]. Initially, a 59.06-inch flowline with a diameter of 1⁄4 inches was established to facilitate the passage of CO_2 gas from the storage cylinder to the Staging Manifold (SM) depicted in Figure 3b, measuring 8 inches in length and 2.16 inches in diameter. Within the SM, the pressure of CO_2 was gradually allowed to increase, reaching post-combustion conditions ranging from 0.15 to 1 bar.

Subsequently, a Reactor (R) housed in a water bath, as shown in Figure 4, was connected to V1 through a 13-inch flow line with a diameter of 1⁄4 inches. Finally, a vacuum pump with a capacity of 1 horsepower was linked to a 47-inch flow line with a diameter of 1⁄4 inches, positioned between the CO_2 storage cylinder and V1. This setup was instrumental in evacuating CO_2 from the flow loop at the conclusion of each sorption cycle conducted at specific pressure and temperature conditions.

During the CO_2 adsorption test: first, the vacuum pump (VP) was used to eliminate air molecules from the airtight apparatus, ensuring the absence of other gases in the system before the

adsorption process. Subsequently, the Dosing Valve (DV) and Bleeding Valve (BV) were closed, while the Inlet Valve (IV) was opened to allow the passage of CO_2 gas. A specific mass of adsorbent (CS – 1.08g, AC – 1.08g) was precisely measured using a weighing balance and placed inside Reactor (V2) to occupy its volume.

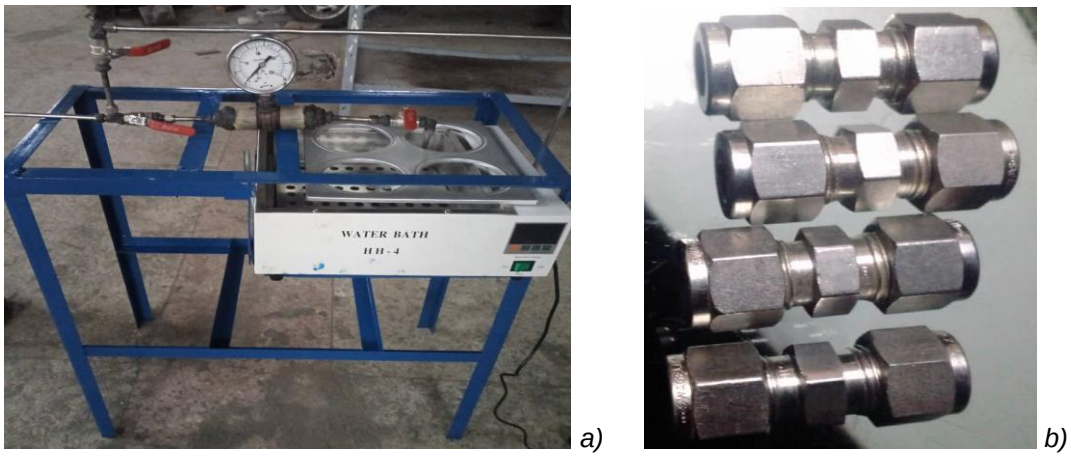

Figure 3. CO_2 adsorption equipment (a)Experimental setup for evaluation of CO_2 adsorption capacity (b) Reactors for storing adsorbents

Slika 3. Oprema za adsorpciju CO_2 (a) Eksperimentalna postavka za procenu kapaciteta adsorpcije CO_2 (b) Reaktori za skladištenje adsorbenata

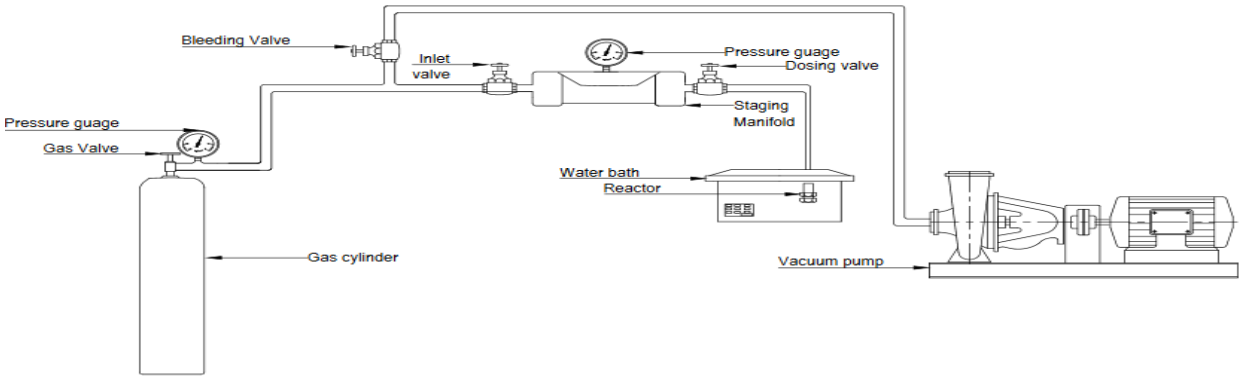

Figure 4. Schematic of CO_2 adsorption experimental setup

Slika 4. Šema eksperimentalne postavke za adsorpciju CO_2

Next, CO_2 gas was gently introduced into the Staging Manifold (V1) from the CO_2 gas cylinder (CGC) while DV and BV were closed, allowing the pressure to build up in V1 to a specific pressure of interest (P1 – 2.0, 3.0, 4.0, 5.0, 6.0, 8.0, 10.0, and 15.0 psi). Once the desired pressure was reached, IV was promptly closed to maintain a constant pressure in V1. The Staging Manifold was sealed for 15 minutes to check for any leakages, which were monitored through any noticeable pressure drop indicated by the Pressure Gauge (PG).

Following this, an equilibration temperature was maintained for 30 minutes. DV was then cautiously opened, allowing CO_2 gas to flow into V2 submerged in a water bath (WB) kept at a specific temperature. This initiated contact with the adsorbents, allowing the adsorption process to occur over a period of 60 minutes. The final pressure, denoted as P2, was recorded by the PG. DV was closed, and BV was opened to enable CO_2 entry from CGC into V1 until the pressure of interest was achieved. This experiment was repeated for each sorption cycle under incremental pressure and constant temperature conditions.

At the end of each sorption cycle, with pressure increment and constant temperature, DV was closed, and V1 was detached from the apparatus. The apparatus was sealed, and residual gas molecules were removed using VP. A specific mass of adsorbent was re-measured and placed in V1, occupying its volume, and the experiment was repeated as described above. The temperatures

utilized in this experiment were 26°C, 40°C, and 70°C, while the pressures of interest were 5 psi, 10 psi, and 15 psi.

2.2.4. RSM Modelling

The RSM modelling involved the examination of two variables from the CO_2 adsorption test: temperature (ranging from 27°C to 40°C) and pressure (ranging from 20 psi to 100 psi) to understand their impact on CO_2 adsorption (measured in mmol/g). These variables were used as input data for the BBD-RSM modelling. The BBD generated 10 experimental runs, which were utilized in the modelling process. Various regression analysis models were assessed to identify the most accurate one that could approximate the experimental data precisely. The outcomes were analysed using 3D response plots and an analysis of variance (ANOVA). The suitability of the model was evaluated through ANOVA, coefficient of determination (R^2), F-value, P-value, and residual analysis. The 2FI model exhibited superior performance and was chosen based on statistical parameters such as R^2, adjusted R^2, predicted R^2, standard deviation, and coefficient of variance (COV). Through multiple regression analyses, these models were fitted to the experimental data, enabling the estimation of responses from independent variables using the provided general equations below. The general form of the 2FI regression model is given as

$$y = a_o + \sum_{i=1}^{k} a_i x_i + \sum_{i=1}^{k} \sum_{j}^{k} a_{ij(i<j)} x_i x_j + e \quad (1)$$

where x_i, x_j, x_l, are the input variables and a_i, a_{ij}, a_{ii}, and a_{ijl} are the coefficient of each of the terms, a_o is the offset and e is the residual or error term.

The statistical metrics which are used to assess the performance of the RSM comprise the coefficient of determination (R^2), the mean-square error (MSE), the root-mean-square error (RMSE), the mean absolute error (MAE), the mean absolute percentage error (MAPE) and the standard deviation as given below

$$R^2 = \frac{\sum_{i=1}^{n}\left(x_{a,i}-x_{p,i}\right)^2}{\sum_{i=1}^{n}\left(x_{p,i}-x_{a,ave}\right)^2} \quad (2)$$

$$MSE = \frac{1}{n}\sum_{i=1}^{n}\left(x_{p,i}-x_{a,i}\right)^2 \quad (3)$$

$$RMSE = \sqrt{\frac{1}{n}\sum_{i=1}^{n}\left(x_{p,i}-x_{a,i}\right)^2} \quad (4)$$

$$MAE = \frac{1}{n}\sum_{i=1}^{n}\left|\left(x_{a,i}-x_{p,i}\right)\right| \quad (5)$$

$$MAPE = \frac{\frac{1}{n}\sum_{i=1}^{n}\left|\left(x_{a,i}-x_{p,i}\right)\right|}{\frac{1}{n}\sum_{i=1}^{n} x_{a,i}} \quad (6)$$

$$std\ dev = \sum_{i=1}^{n}\frac{(x_{di}-m)^2}{n-1} \quad (7)$$

where n is the number of experimental runs, xp,i is the estimated values, xa,i is the experimental values, xa,ave is the average experimental values, x_{di} is the difference between the actual and estimated value, m is the mean value of x_d dataset, k is the number of input variables.

3. RESULTS AND DISCUSSION

3.1. PPAC Characterization Result

The SEM image depicted in figure 5 shows the morphology of the PPAC at 500µm.

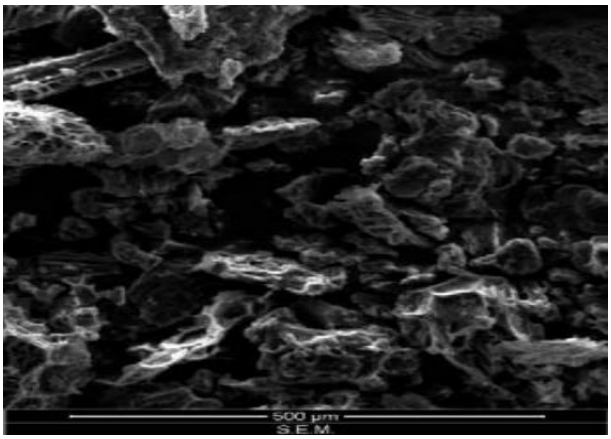

Figure 5. SEM images of PPAC

Slika 5. SEM slike PPAC-a

The morphology of PPAC from in 5 shows irregular sponge-like protrusions distributed unevenly, with well-defined pores. These protrusions are indicative of the organic content present in plantain peels, while the clearly visible pores are the outcome of thermal and chemical treatments, involving processes like carbonization and activation. These treatments removed volatile components from the sample, resulting in the distinctive microstructure observed in PPAC. This microstructure signifies an enhanced surface area, essential for effective adsorption of gaseous substances.

The EDX analysis depicted in Figure 6 reveals the elemental composition of PPAC, indicating the presence of oxygen (20.23 wt%), carbon (33.4 wt%), potassium (5.32 wt%), magnesium (1.35 wt%), calcium (4.50 wt%), silicon (30.0 wt%), and iron (5.20 wt%). The predominant components in PPAC are carbon, silicon, and oxygen, with lower proportions of potassium, iron, calcium, and magnesium, each decreasing in percentage weight. The oxygen content in PPAC holds critical significance, as oxygen functional groups play a pivotal role in determining the surface properties of carbons, influencing their suitability as ion exchangers, adsorbents, etc.

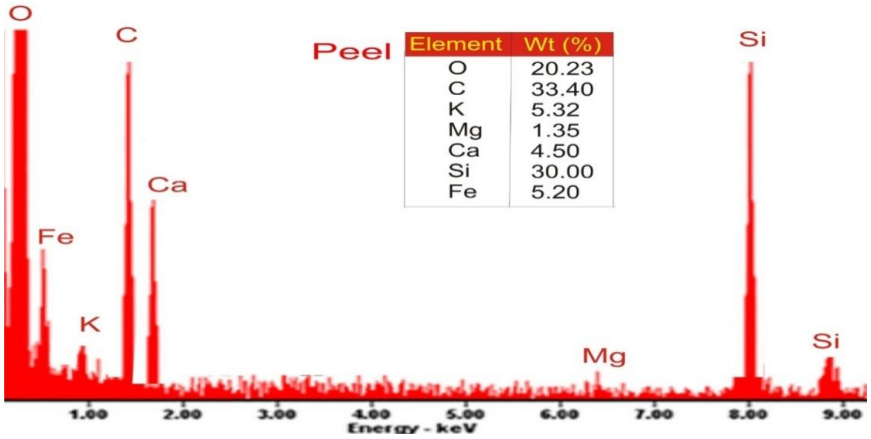

Figure 6. EDX analyses showing the chemical composition of PPAC

Slika 6. EDX analize koje pokazuju hemijski sastav PPAC-a

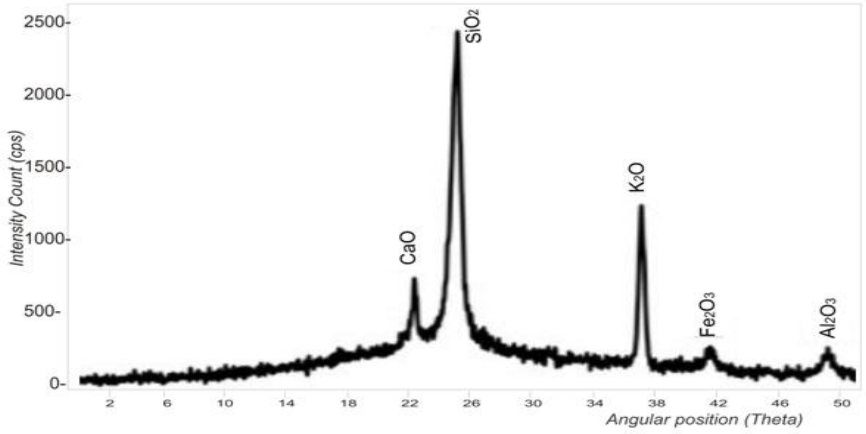

Figure 7. XRD analyses results of PPAC

Slika 7. Rezultati XRD analize za PPAC

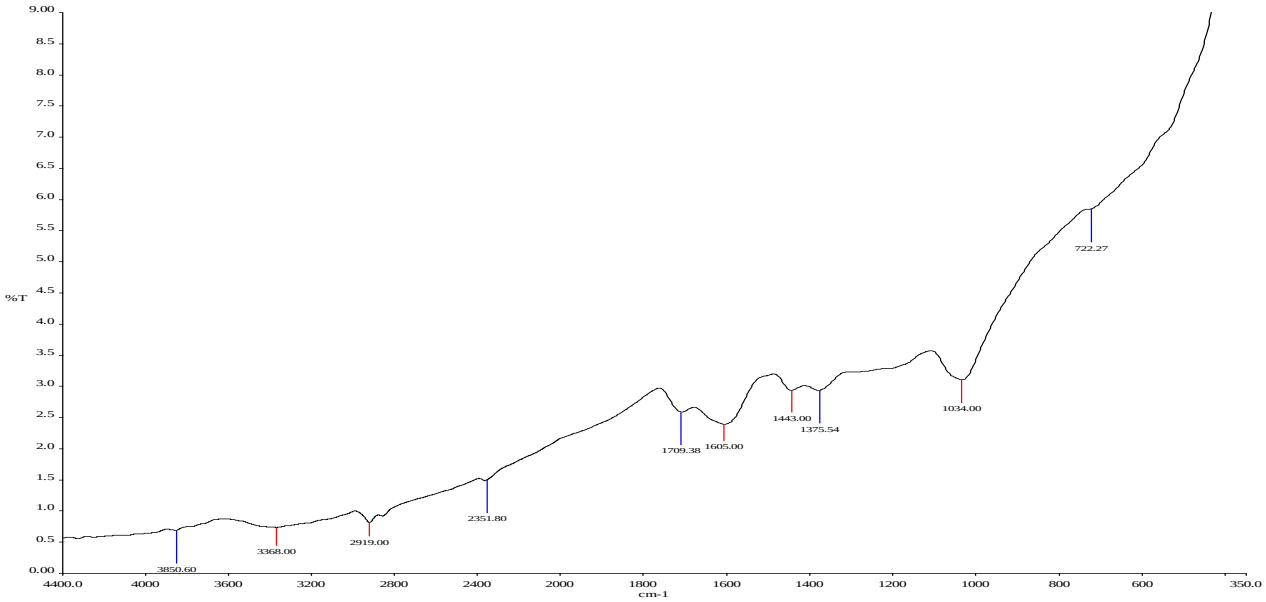

Figure 8. FTIR analyses of PPAC

Slika 8. FTIR analize PPAC

The XRD results of the PPAC shown in Figure 7 reveal the crystallinity of the and hence indicate the oxide composition of the PPAC. Diffraction angles were observed within the range of 0 to 51.6°. Prominent peaks were identified at 22°, 25°, and 36.5°, while minor peaks were noted at 42° and 49°. The major peaks indicate the presence of silicon oxide (SiO_2) as the predominant component in PPAC, followed by potassium oxide (K_2O) and calcium oxide (CaO). Additionally, the minor peaks suggest the existence of iron (III) oxide (Fe_2O_3) and aluminium oxide (Al_2O_3). The prevalence of these oxides, particularly SiO_2, K_2O, and CaO in PPAC, signifies the transformation of activated carbon from its precursors due to the thermal and chemical treatments applied during its preparation

The FTIR analysis of PPAC, as depicted in figure 8, displayed peaks at specific wavenumbers: 3850.60 cm^{-1}, 3368 cm^{-1}, 2919 cm^{-1}, 2315.8 cm^{-1}, 1709.38 cm^{-1}, 1605 cm^{-1}, 1443 cm^{-1}, 1375.54 cm^{-1}, 1034 cm^{-1}, and 722.27 cm^{-1}. Bands within and above 3850 cm^{-1} signified OH stretching vibrations, while those within the range of 3500-3860 cm^{-1} indicates OH stretching of proteins or polyphenols. Bands between 3300-3500 cm^{-1} represented bonded N-H/C-H/O-H stretches typical of amines and amides. Aliphatic stretches involving C-H and $C-H_2$ bonds were denoted by bands in the 2850-2950 cm^{-1} range. The presence of C-N bonds was indicated by bands around 2100-2350 cm^{-1}. Double bonds of C=O, characteristic of ketones, were noted within the 1700-1750 cm^{-1} range. Inorganic carbonate groups (-C=O groups) were identified in the 1400-1470 cm^{-1} range, while CH and CH_2 aliphatic bending groups were present in the 1350-1440 cm^{-1} range. Silica was evidenced by the bands at 1054 cm^{-1}, and out-of-plane CH bending was observed in the 700-800 cm^{-1} range.

The specific surface area and pore size distribution of PPAC were determined through BET and BJH analyses. The BET analyses revealed a surface area of 1062.350 m²/g. Additionally, the adsorption and desorption average pore widths were found to be 28.25Å and 28.22Å, respectively, as per the BET analyses. On the other hand, the BJH analyses indicated average pore widths of 28.55Å (adsorption) and 30.55Å (desorption). The single-point adsorption total pore volume of pores measured 0.554500 cm³/g, whereas the desorption cumulative volume of pores was 0.452220 cm³/g. The isotherm linear plot for the BET/BJH analyses is presented in figure 9.

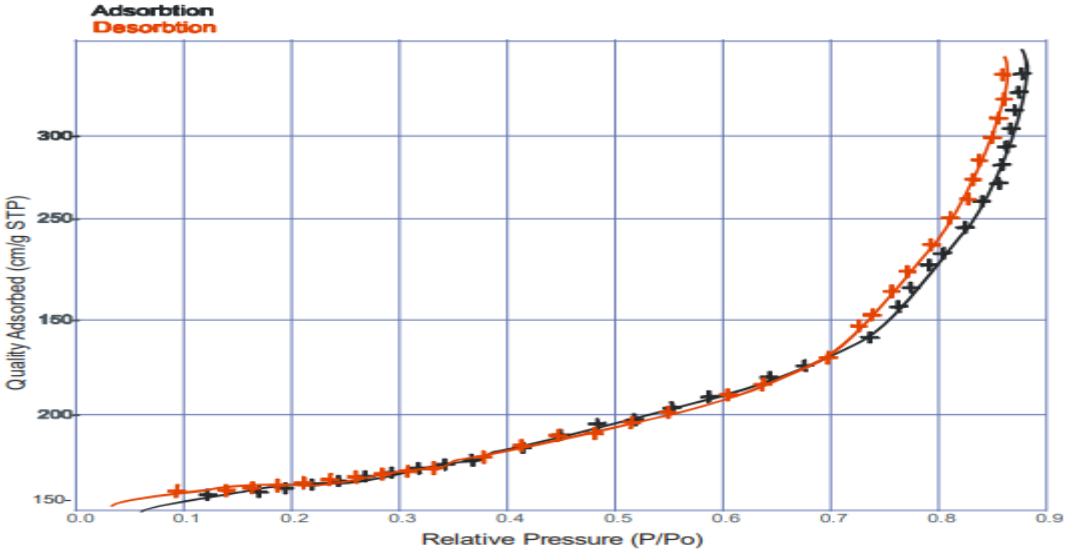

Figure 9. Isotherm linear plot of the PPAC subjected to BET/BJH analyses

Slika 9. Izotermni linearni dijagram za PPAC podvrgnut BET/BJH analizama

From figure 9 shows that the quality of absorbed species from the PPAC would increase exponentially with increase in the relative pressure (P/Po)

3.2. Results for CO_2 Adsorption

CO_2 adsorption results are given for PPAC samples of 150µm and 845µm. For the 150µm PPAC sample, the CO_2 adsorption capacities were found to be 2.1558 mmol/g and 9.6126 mmol/g at pressures of 20 psi and 100 psi, respectively, and at an adsorption temperature of 27°C. However, at 40°C, the CO_2 adsorption capacities at 20 psi and 100 psi were recorded as 1.4438 mmol/g and 7.7154 mmol/g, respectively. Figure 10 illustrates the differences in both the final adsorption pressure and CO_2 adsorption capacity for different temperatures under the same applied initial

pressures. The CO_2 adsorption capacity as a function of initial and final pressures is depicted in figures 10a and 10b for 27°C and 40°C, respectively.

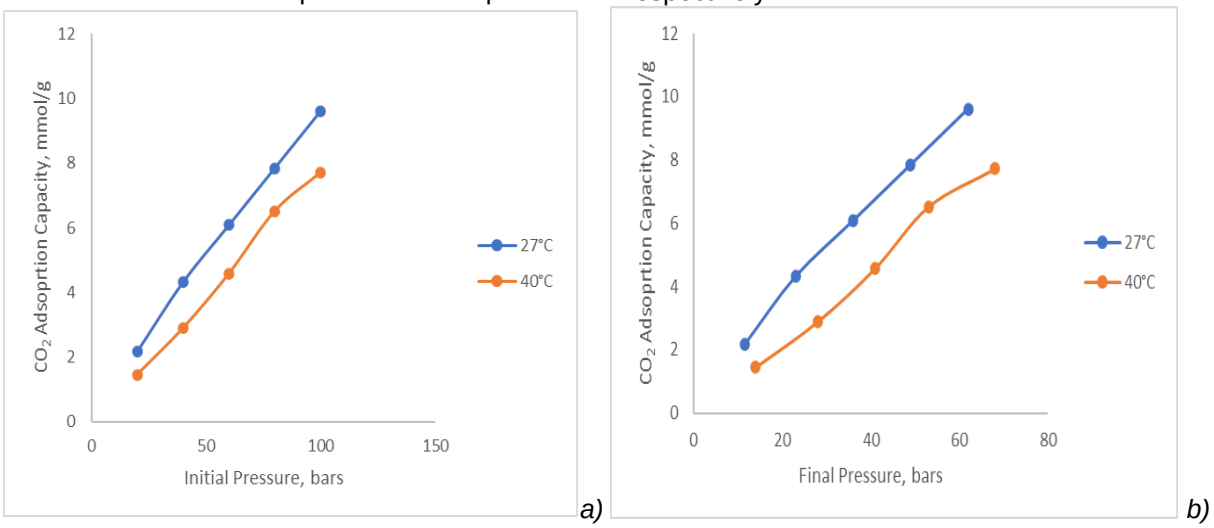

Figure 10. CO_2 adsorption capacities for 150µm (a) as a function of Initial pressure (b) As a function of final pressure

Slika 10. Kapaciteti adsorpcije CO_2 za 150µm (a) u funkciji početnog pritiska (b) u funkciji konačnog pritiska

As shown in Figure 10, it is evident that the CO_2 adsorption capacity rises with increasing pressures, both initial and final. However, at 27°C, the PPAC exhibited a higher CO_2 adsorption capacity compared to that at 40°C, as pressures were varied. This indicates that for the 150µm activated carbon, CO_2 adsorption decreased with an increase in adsorption temperature. The increased CO_2 adsorption observed at the higher temperature of 150µm PPAC is attributed to the greater pressure drop across the membrane material at lower temperatures. This condition created a stronger driving force, leading to higher CO_2 adsorption, as illustrated in Figure 11.

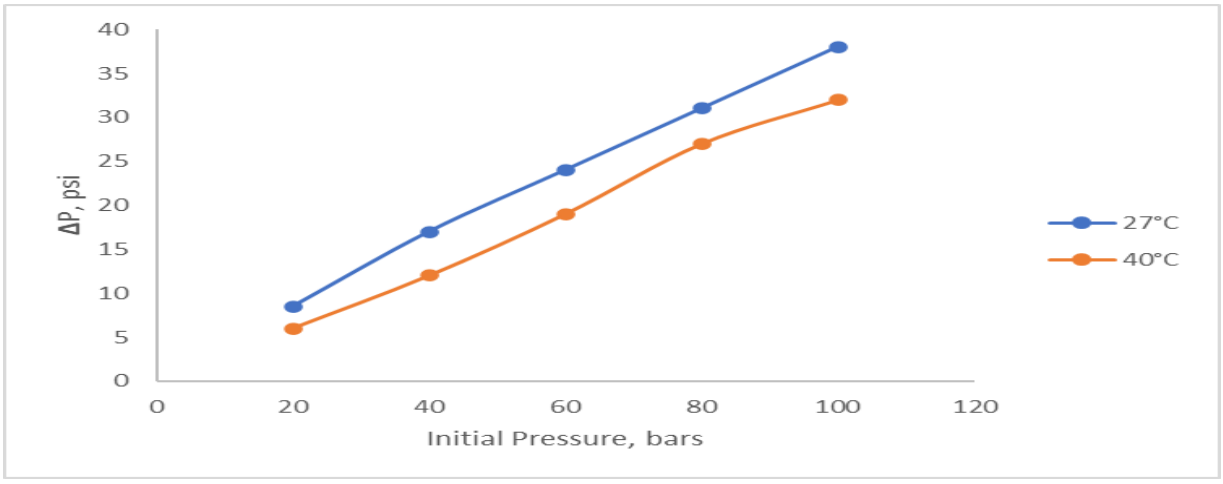

Figure 11. Pressure drop across PPAC for various adsorption temperatures

Slika 11. Pad pritiska na PPAC za različite temperature adsorpcije

Figure 11 reveals that with an increase in temperature, the pressure drop across the PPAC material diminishes, leading to a lower CO_2 adsorption capacity. The pressure drop refers to the disparity between the final resultant pressure and the initial pressure applied across the activated carbon material. The driving force for gas adsorption is intricately linked to the difference in partial pressure of the gas across the adsorbent material. A higher-pressure drop indicates a more

substantial difference in CO_2 partial pressure, thereby facilitating more significant adsorption.

For the 845µ PPAC sample, the CO_2 adsorption capacities were 2.542 mmol/g and 12.7103 mmol/g at 20 psi and 100 psi pressures, respectively, at 27°C temperature. At 40°C temperature, the CO_2 adsorption capacities were 3.6775 mmol/g and 8.451 mmol/g at 20 psi and 100 psi pressures, respectively. Figure 12 shows the CO_2 adsorption capacities as a function of the initial and final pressures for the 845µm PPAC.

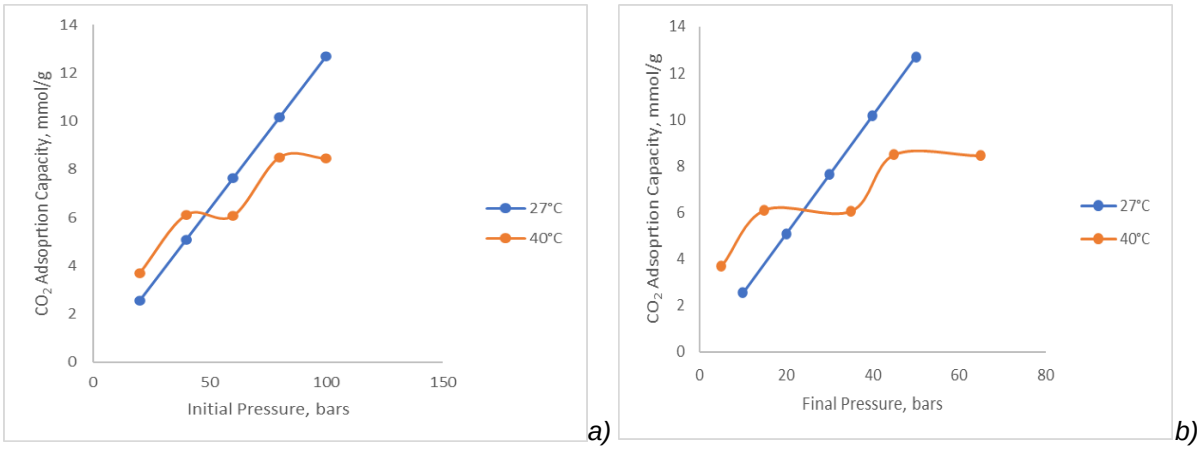

Figure 12. CO_2 adsorption capacities for 845µm (a) as a function of Initial pressure (b) As a function of final pressure

Slika 12. Kapacitet adsorpcije CO_2 za 845µm (a) kao funkcija početnog pritiska (b) Kao funkcija konačnog pritiska

The CO_2 adsorption capacities of 845µm size PPAC exhibit variations with temperature and pressure. At 27°C, the CO_2 adsorption capacity of 845µm PPAC demonstrated a linear increase with both initial and final pressures. The initial pressure corresponds to the applied inlet pressure of the feed CO_2, while the final pressure corresponds to the recorded pressure of the adsorbed CO_2 species. Conversely, at 40°C adsorption temperature, the CO_2 adsorption displayed an erratic trend. The adsorption showed both increasing and decreasing patterns with both applied and final pressures. CO_2 adsorption increased between inlet pressures of 20 psi to 40 psi and then decreased between 40 psi and 60 psi pressures. It then increased again from 60 psi to 80 psi pressures and subsequently decreased between 80 psi and 100 psi pressures.

Figure 13 shows the comparison of the CO_2 adsorption capacities of the PPAC for the 150µm and 845µm at several pressures and temperatures.

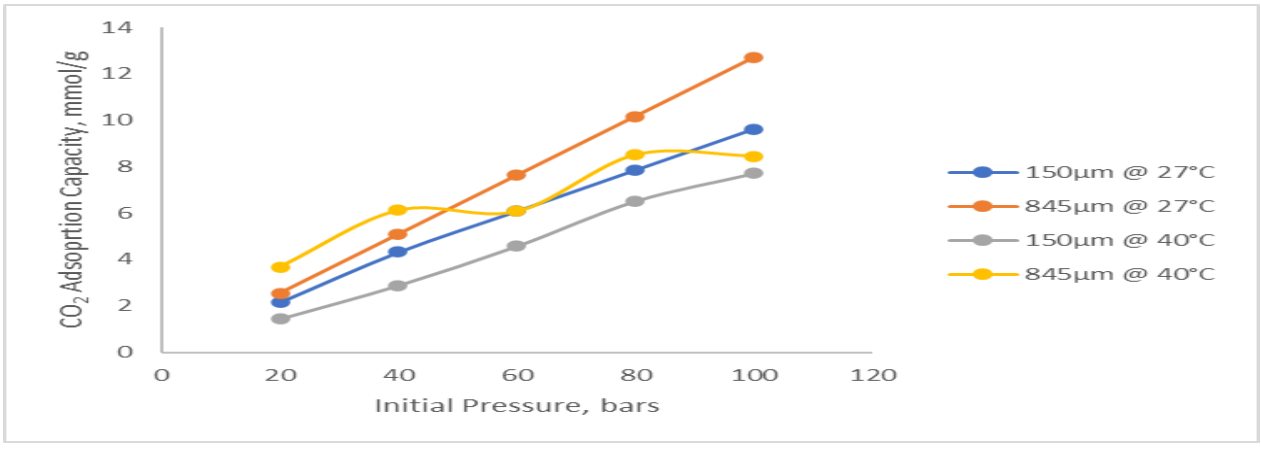

Figure 13. CO_2 adsorption capacities at several particle sizes of PPAC

Slika 13. Kapacitet adsorpcije CO_2 pri nekoliko veličina čestica PPAC-a

From figure 13, it is observed that CO_2 adsorption exhibited higher values for 845µm particles compared to 150µm particles. This finding indicates that CO_2 adsorption increases with larger particle size of activated carbon, a trend consistent across both 27°C and 40^{o}C adsorption temperatures. Several factors contribute to this phenomenon:

Activated carbon materials possess a porous structure, characterized by a network of tiny pores and a high surface area. Larger particle sizes provide more space for these pores, creating a greater surface area available for adsorption. Consequently, larger particles offer ample room for CO_2 molecules to be adsorbed onto the surface of the activated carbon. In contrast, smaller particles result in crowded pores, limiting the accessibility of CO_2 molecules to the interior of the pores.

Furthermore, smaller particles tend to impede the diffusion of CO_2 molecules into the internal pores due to increased resistance. Larger particles, on the other hand, offer open pathways for CO_2 molecules to enter the porous structure, enhancing adsorption capacity. Additionally, larger particles provide a greater number of active adsorption sites due to their larger surface area. This abundance of adsorption sites allows for more interactions between CO_2 molecules and the adsorption sites, resulting in a higher adsorption capacity.

In contrast, smaller particles tend to agglomerate, reducing the overall surface area available for adsorption. Larger particles, being less prone to agglomeration, maintain a larger accessible surface area for CO_2 adsorption, facilitating faster and more efficient adsorption and mass transfer of CO_2 molecules. These characteristics collectively contribute to the observed increase in CO_2 adsorption capacity with larger particle size of activated carbon.

4.2. RSM Modelling Results

The RSM model was developed by fitting the experimental data to the RSM model. The 2FI model gave the highest fit to the actual data and was selected. The equation for the 2FI model generated by RSM is given as

$$Y = +5.32 - 0.6858X_1 + 3.46X_2 - 0.22721X_1X_2 \quad (8)$$

Equation 8 generated by RSM shows CO_2 adsorption represented as Y while temperature and pressure are represented by X_1 and X_2 respectively. The equation 7 shows that CO_2 adsorption is affected by temperature and pressure of the CO_2 gas. Equation 8, expressed in terms of the actual factors, provides a tool for predicting the response for specific levels of each factor. To use this equation effectively, the levels must be specified in the original units of each factor for both input parameters and the response variable.

The RSM model demonstrated strong predictive capability, proven by high coefficients of determination (R^2=0.9973, Adjusted R^2=0.9959, and predicted R^2=0.9909). R^2 values exceeding 0.8 typically indicate a significant fit between experimental and model-predicted results. The low coefficient of variance (CV) at 3.24% highlights the reliability of the experiment. The results from the analysis of variance (ANOVA), summarized in Table 1, confirmed the significance of the input parameters and the 2FI model. In the 2FI model, each term was assessed for significance using p-values at a confidence level of 95%. Terms with p-values less than or equal to 0.05 were considered significant, indicating their impact on the response. Additionally, higher F-values for model terms highlighted their substantial influence on the response variable. Notably, the p-value less than 0.0001 and the f-value of 731.21 further validate the acceptability of the 2FI model.

Table 1. Model coefficient based on ANOVA

Tabela 1. Koeficijent modela na osnovu ANOVA

Source	Sum of Squares	df	Mean Square	f-value	p-value	
Model	64.9	3	2.63	731.21	<0.0001	Significant
A-Temperature	4.7	1	4.7	158.97	<0.0001	
B-Pressure	59.94	1	59.94	2025.92	<0.0001	
AB	0.2581	1	0.2581	8.73	0.0255	
Residual	0.1775	6	0.0296			
Cor Total	65.08	9				

Figure 14 shows the actual vs. predicted response for the reduced cubic regression model.

In Figure 14a, the actual and predicted values are closely aligned and exhibit good agreement, as indicated by their proximity to the 45° line. Figure 14b illustrates the graphical analysis of the model through a normal plot of residuals. The majority of data points fall within the range of 1.0 and -1.0

when represented as residuals. This alignment along a straight line suggests a normal distribution of residuals as the focus progresses. Equation (8) has proven to be the most suitable model for interpreting historical data related to CO_2 adsorption responses. The model highlights that all independent parameters significantly influence the response parameter.

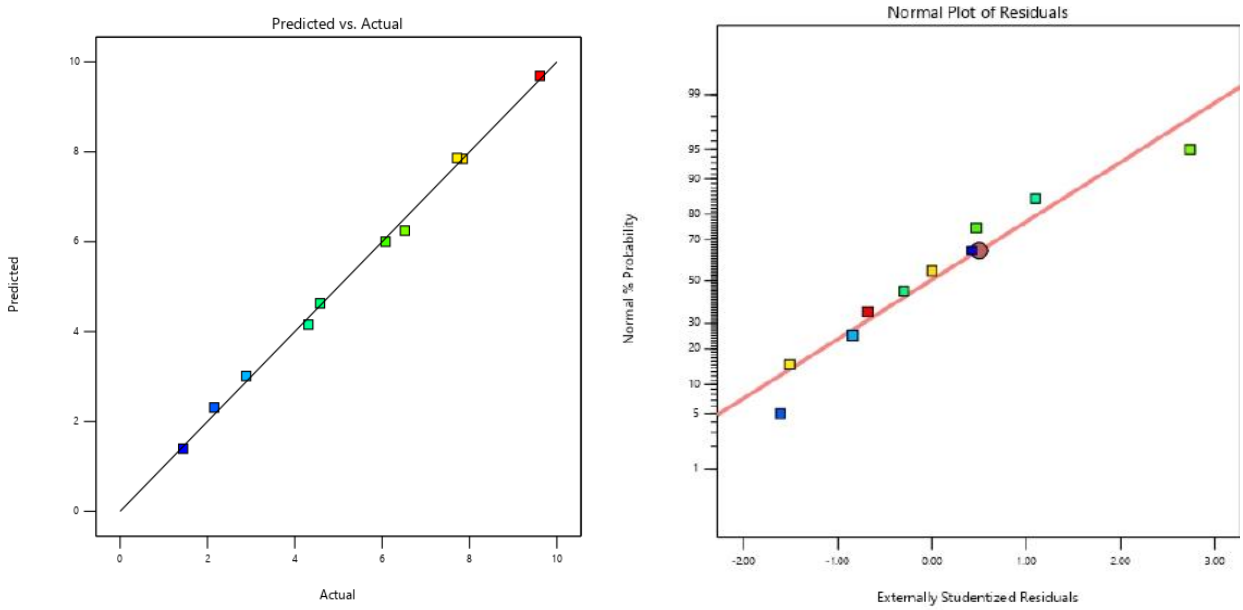

a) *b)*

Figure 14. RSM diagnostic plots: a) Predicted vs actualm b) Normal plot of residuals

Slika 14. RSM dijagnostički grafici: a) Predviđeni naspram stvarnih (b) Normalni grafikon reziduala

Table 2. Actual and predicted results for CO_2 adsorption

Tabela 2. Stvarni i predviđeni rezultati za adsorpciju CO_2

Run	Temperature ^oC	Pressure psi	CO_2 Adsorption, mmol/g	
			Actual	Predicted
1	27	20	2.16	2.31
2	27	40	4.31	4.16
3	27	60	6.08	6
4	27	80	7.85	7.85
5	27	100	9.61	9.69
6	40	20	1.44	1.39
7	40	40	2.89	3.01
8	40	60	4.58	4.63
9	40	80	6.52	6.25
10	40	100	7.72	7.86

Table 3 shows the performance metrics for the RSM model.

Table 3 shows that the RSM model provided accurate predictions of the experimental data based on the considered error metrics. The R^2 values exceeding 0.9 indicate highly accurate predictions of the test data. The low MSE (0.017) and RMSE (0.13) values signify minimal errors between the actual data and the predicted response. Additionally, the MAE (0.109) and MAPE (2.72) values emphasize the high accuracy of the predictions.

Table 3. Performance metrics for RSM indicating model validation

Tabela 3. Metrika performansi za RSM koja ukazuje na validaciju modela

Parameter	**Result**
MSE	0.01697
RMSE	0.130269
MAE	0.109
MAPE	2.7244
R^2	0.9973
Adjusted R^2	0.9959
Predicted R^2	0.9909
CV	3.24
Adeq Precision	76.26
Std Dev.	0.172

The reliability of the model and fit are further supported by its low C.V. % value (3.34%), indicating a strong correlation between the actual

and expected values. Adeq Precision, which measures the signal-to-noise ratio, is desirable when greater than 4. The Adeq Precision value of 76.262 signifies a robust signal. This model is well-suited for navigating the design space. The optimization conducted using RSM resulted in optimized values for temperature, pressure, and CO_2 adsorption at 27°C, 100 bars, and 9.69 mmol/g, respectively.

4. CONCLUSION

Comprehensive investigation of activated carbon derived from ripe plantain peels has been achieved. Through carbonization and activation with H_3PO_4, plantain-peel activated carbon (PPAC) was created and extensively analysed. Characterisation tests, CO_2 adsorption test and RSM modelling were performed. The characterisation reveals that PPAC was effective for CO_2 adsorption as evidenced by the SEM analyses, XRD analyses, FTIR analyses, BET and BJH analyses etc. CO_2 adsorption (mmol/g) increased with increasing pressures (both initial and final). However, at 27°C, PPAC exhibited higher CO_2 adsorption capacity than at 40°C for the same pressure range. This suggests that CO_2 adsorption decreased with increasing adsorption temperature. The higher CO_2 adsorption at lower temperatures (27°C) was attributed to a higher pressure drop across the PPAC material. The pressure drop difference served as a driving force for enhanced CO_2 adsorption. Comparing two particle sizes (150µm and 845µm) of PPAC, CO_2 adsorption capacity was higher for larger particle size (845µm). Larger particles offered more surface area, better pore accessibility, and facilitated faster mass transfer, resulting in increased adsorption capacity.

From the Response Surface Methodology (RSM) model, the developed 2FI model demonstrated exceptional accuracy, as observed by high coefficients of determination (R^2=0.9973) and low error metrics (MSE=0.01697, RMSE=0.130269, MAE=0.109, MAPE=2.7244). The reliability of the model was confirmed by the Adeq Precision value of 76.26. Utilizing the optimized model. The optimisation conducted using RSM determined the optimal values for CO_2 adsorption as 9.69 mmol/g at temperature and pressure values of 27°C, 100 bars respectively. Generally, PPAC demonstrated favourable characteristics for CO_2 adsorption, making it a promising solution for mitigating CO_2 emissions and addressing climate change challenges.

Acknowledgement

Special recognition goes to TETFUND for the funding that enabled this was to be accomplished.

5. REFERENCES

[1] A.H.Jagaba, I.M.Lawal, A.A.Ghfar, A.K.Usman, N.S. Yaro, Noor, A.HBirniwa (2023) Biochar-based geopolymernanocomposite for COD and phenol removal from agro-industrial biorefinery wastewater: Kinetic modelling, microbial community, and optimization by response surface methodology. *Chemosphere*, *339*, 139620. doi: 10.1016/j. chemosphere. 2023.139620

[2] C.U.Uzoho, I.F.Okorafor, D.O.Olomu, N.E.Achilike, O.D.Adesina, M.O.Onyekonwu (2023) Determination of Minimum Miscibility Pressure Between Heavy Oil–Supercritical Carbon Dioxide System Using the Slim Tube Method. In *SPE Nigeria Annual International Conference and Exhibition* (p. D021S002R001). SPE.

[3] A.H.Jawad, A.S.Abdulhameed, T.A.Khadiran, Z.A. Othman, L.D.Wilson, S.Algburi (2023) Response surface methodology for optimizing methylene blue dye removal by mesoporous activated carbon derived from renewable woody Bambusoideae waste. *Int. J. of Phytoremediation*, 26(5), 727-739, doi: 10.1080/15226514.2023.2262040.

[4] C.Owusu, E.A.Mends, G.Acquah (2022) Enhancing the physical qualities of activated carbon produced from palm kernel shell via response surface methodology—process variable optimization. *Biomass Conversion and Biorefinery*, ID 254561779, doi:10.1007/s13399-022-03595-7

[5] Z.Khoshraftar, H.Masoumi, A.Ghaemi (2023) Characterization and evaluation of low-cost biomass-based-AC for CO_2 capture: A review. Case Studies in Chemical and Environmental Engineering, 100373. http://dx.doi.org/10. 1016/ j.cscee.2023.100373

[6] G. Greco, R.L.Canevesi, C.Di Stasi, A.Celzard, V. Fierro, J.J. Manya (2022) Biomass-derived carbons physically activated in one or two steps for CH4/CO2 separation. *Renewable Energy*, *191*, 122-133, doi: 10.1016/j.renene.2022.04.035

[7] M.M.Bade, A.A.Dubale, D.F.Bebizuh, M. Atlabachew (2022) Highly efficient multisubstrate agricultural waste-derived activated carbon for enhanced CO2 Capture. *ACS omega*, *7*(22), 18770-18779, https://doi.org/10.1021/acsomega.2c01528

[8] J.A.Sosa, J.R.Laines, D.S.García, R.Hernández, M. Zappi, A.E. de los Monteros (2023) Activated Carbon: A Review of Residual Precursors, Synthesis Processes, Characterization Techniques, and Applications in the Improvement of Biogas. *Environmental Engineering Research*, *28*(3), 220100, https://doi.org/10.4491/eer.2022.100

[9] A.Inam, S.S.Oncel (2021) Photobioreactors as potential tools for environmentally friendly and sustainable buildings. *International Journal of Environmental Science and Technology*, 19(4), 1-12, http://dx.doi.org/10.1007/s13762-021-03281-7

[10] Z.Khoshraftar, A.Ghaemi (2022) Evaluation of pistachio shells as solid wastes to produce activated carbon for CO_2 capture: isotherm, response surface methodology (RSM) and artificial neural network (ANN) modeling. *Current Research in Green and Sustainable Chemistry*, *5*, 100342, https://doi.org/10.1016/j.crgsc.2022.100342.

[11] M.Gorbounov, B.Petrovic, S.Ozmen, P.Clough, S.M.Soltani (2023) Activated carbon derived from Biomass combustion bottom ash as solid sorbent for CO_2 adsorption. *Chemical Engineering Research and Design*, *194*, 325-343, https://doi.org/10.1016/j.cherd.2023.04.057

[12] A.Dey, B.Saini, S.C.Balchandani, S.K.Dash (2022) Investigation of equilibrium CO_2 solubility in 35 wt% aqueous 1-(2-aminoethyl) piperazine (AEP) and performance study over monoethanolamine for CO2 absorption. *Materials Today: Proceedings*, *61(2)*, 498-503, http://dx.doi.org/10.1016/ j.matpr. 2021.12.357

[13] Y.Yang, C.Zhu, Q.Huang (2021) Progress on preparation and adsorption application of solid waste derived hierarchical porous carbon. Chemical Industry and Engineering Progress, 40(1), 427-439, doi, 10.16085/j.issn.1000-6613.2020-0439.

[14] H.Yang, C.He, L.Fu, J.Huo, C.Zhao, X.Li, Y.Song (2021) Capture and separation of CO_2 on BC3nanosheets: A DFT study. *Chinese Chemical Letters*, *32*(10), 3202-3206, http://dx.doi.org/10. 1016/ j.cclet.2021.03.038

[15] S.Janakiram, J.L.M.Espejo, K.K.Høisæter, A. Lindbråthen, L.Ansaloni, L.Deng (2020) Three-phase hybrid facilitated transport hollow fiber membranes for enhanced CO2 separation. *Applied Materials Today*, *21*, 100801,https://doi.org/10. 1016/j.apmt.2020.100801

[16] Y.Bao, J.Li, Q.Guo, B.Jiang, C.Su (2022) Review on technologies of geological resources exploitation by using carbon dioxide and its synchronous storage. Coal Science and Technology, 50(6), 84-95. doi : 10.13199/j.cnki. cst.2021-0552.

[17] Y.Devarajan, N.Lakshmaiya (2022) Effective utilization of waste banana peel extracts for generating activated carbon-based adsorbent for emission reduction. Biomass Conversion and Biorefinery, 1-7, http://dx.doi.org/10.1007/s13399-022-03470-5

[18] J.Maharjan, V.K.Jha (2022) Activated carbon obtained from banana peels for the removal of As (III) from water. Scientific World, 15(15), 145-157, https://doi.org/10.3126/sw.v15i15.45665

[19] H.Patel, H.Weldekidan, A.Mohanty, M.Misra (2023) Effect of physicochemical activation on CO_2 adsorption of activated porous carbon derived from pine sawdust. Carbon Capture Science Technology, 8, 100128, https://doi.org/10. 1016/ j.ccst.2023.100128

[20] J.Serafin, M.Ouzzine, C.Xing, H.El Ouahabi, A. Kamińska, J.Sreńscek-Nazzal (2022) Activated carbons from the Amazonian biomass andiroba shells applied as a CO_2 adsorbent and a cheap semiconductor material. Journal of CO2 Utilization, 62,102071,https://doi.org/10.1016/j.jcou.2022. 102071

[21] I.Yanti, P.P.Sationo, W.F.Winata, M.Anugrahwati, A.K.Anas, Y.A.Swasono (2023) Effectiveness of activated carbon magnetic composite from banana peel (Musa acuminata) for recovering iron metal ions. Case Studies in Chemical and Environmental Engineering, 8(4), 100378, http://dx.doi.org/ 10. 1016/j.cscee.2023. 100378

[22] K.Jasri, A.S.Abdulhameed, A.H.Jawad, Z.A. ALOthman, T.A.Yousef, O.K.Al Duaij. (2023) Mesoporous activated carbon produced from mixed wastes of oil palm frond and palm kernel shell using microwave radiation-assisted K2CO3 activation for methylene blue dye removal: Optimization by response surface methodology. Diamond and Related Materials, 131, 109581, https://doi.org/10. 1016/j.diamond.2022.109581

[23] Y.Vasilev, P.Vasileva, A.Tsvetkova (2020) The Study of Spreading Information on Carbon Capture, Utilization and Storage Technologies in the Social Media. 20th International Multidisciplinary Scientific GeoConference Proceedings SGEM, 20(5), 833-839, http://dx.doi.org/10.5593/sgem2020/5.1/s20. 105

[24] Y.Li, G.Zhang, J.Liu, G.Li, Y.Wang (2023) Optimized preparation of multi-matrix activated carbon for CO_2 capture by response surface methodology: The advantages of co-pyrolysis of biomass and plastics. J. of the Energy Institute, 101415, doi:10.1016/j.joei.2023.101415

[25] M.Ounis, E.Sanz-Santos, F.Fakhfakh, M.K. Younes, B.Hadrich, S.Álvarez-Torrellas, J.García (2023) Optimisation of Adsorption Removal of Bisphenol A Using Sludge-Based Activated Carbons: Application of Response Surface Methodology with a Box–Behnken Design. Arabian Journal for Science and Engineering, 49(3), 1-18, doi:10.1007/s13369-023-08203-y

[26] J.Fito, S.Tibebu, T.T.Nkambule (2023) Optimization of Cr (VI) removal from aqueous solution with activated carbon derived from Eichhorniacrassipes under response surface methodology. BMC chemistry, 17(1), 4, https://doi.org/10.1186/s13065-023-00913-6

[27] Z.Tariq, Z.Xu, M.Gudala, B.Yan, S.Sun (2023 January). Deep-Learning-Based Surrogate Model to Predict CO_2 Saturation Front in Highly Heterogeneous Naturally Fractured Reservoirs: A Discrete Fracture Network Approach. In SPE Reservoir Characterisation and Simulation Conference and Exhibition? (p. D021S007R006). SPE. https://doi.org/10.2118/212658-ms

[28] S.Kumar, K.Prasad, J.M.Gil, A.J.Sobral, J.Koh (2018) Mesoporous zeolite-chitosan composite for enhanced capture and catalytic activity in chemical fixation of CO2. Carbohydrate Polymers, 198, 401-406, https://doi.org/10.1016/j.carbpol.2018.06.100

[29] D.Chaturvedi, O.P.Misra (2019) Modeling impact of varying pH due to carbondioxide on the dynamics of prey–predator species system. Nonlinear Analysis: Real World Applications, 46, 374-402, https://doi.org/10.1016/j.nonrwa.2018.09. 024

[30] A.Mukherjee, B.Saha, C.Niu, A.K.Dalai (2022) Preparation of activated carbon from spent coffee

grounds and functionalization by deep eutectic solvent: Effect of textural properties and surface chemistry on CO2 capture performance. Journal of Environmental Chemical Engineering, 10(6), 108815, http://dx.doi.org/10.1016/j.jece.2022. 108815

[31] N.H.Sabri, N.H.A.Rani, N.F.Mohamad, N.M. Muhsen, M.M.Zaini (2023) Simulation of CO2 capture for amine impregnated activated carbon-palm kernel shell (AC-PKS) adsorbent in pressure swing adsorption (PSA) using Aspen Adsorption. Materials Today: Proceedings, https://doi.org/10.1016/j.matpr.2022.12.206

[32] H.Vogtenhuber, R.Hofmann, F.Helminger, G. Schöny (2018) Process simulation of an efficient temperature swing adsorption concept for biogas upgrading. Energy, 162, 200-209, doi: 10.1016/ j.energy.2018.07.193

[33] R.Maniarasu, S.K.Rathore, S.Murugan (2023) Biomass-based activated carbon for CO2 adsorption–A review. Energy & Environment, 34(5), 1674-1721, doi: 10.1177/0958305X221093465

[34] A.Helmi, F.Gallucci, M. van Sint Annaland. (2014) Resource scarcity in palladium membrane applications for carbon capture in integrated gasification combined cycle units. International journal of hydrogen energy, 39(20), 10498-10506, https://doi.org/10.1016/j.ijhydene.2014.05.009

IZVOD

ISTRAŽIVANJE UČINKA AKTIVNOG UGLJA DOBIJENOG IZ KORE ZRELE BANANE ZA HVATANJE CO_2: MODELIRANJE I OPTIMIZACIJA KORIŠĆENJEM METODOLOGIJE POVRŠINE ODGOVORA

Ova studija istražuje potencijal aktivnog uglja dobijenog iz kore zrele banane (PPAC) za hvatanje ugljen-dioksida (CO_2). PPAC je pripremljen karbonizacijom i aktivacijom pomoću H_3PO_4, a njegova jedinstvena svojstva su opsežno okarakterisana što je otkrilo nepravilne izbočine nalik sunđeru i dobro definisane pore pod skenirajućom elektronskom mikroskopijom (SEM). Elementarna analiza identifikovala je ugljenik, silicijum i kiseonik kao glavne komponente, što je potvrđeno analizom rendgenske difrakcije (XRD) koja ukazuje na prisustvo silicijum oksida (SiO_2), kalijum oksida (K_2O) i kalcijum oksida (CaO). Fourier Transform Infrared (FTIR) spektroskopija je istakla različite funkcionalne grupe na površini PPAC-a. Testovi adsorpcije CO_2 su sprovedeni na 27°C i 40°C sa različitim pritiscima na PPAC čestice veličine 150μm i 845μm. Rezultati su otkrili da se kapacitet adsorpcije CO_2 povećava sa eskalirajućim pritiscima. Izvanredno, na 27°C, PPAC je pokazao superiorne performanse nego na 40°C, što se pripisuje većem padu pritiska koji povećava pokretačku snagu za adsorpciju CO_2. Veće čestice (845 μm) su pokazale veći kapacitet adsorpcije zbog povećane površine, poboljšane dostupnosti pora i bržeg prenosa mase. Sprovedena metodologija površine odgovora (RSM) dala je 2FI model kao najreprezentativniji od projektnih podataka i pokazala je visoku tačnost (R2=0,9973) i nisku metriku greške (MSE=0,01697, RMSE=0,130269, MAE=0,109, MAPE=2,7244). Vrednost Adek Precision od 76,26 potvrdila je pouzdanost modela. Optimizacija korišćenjem RSM-a je dala optimalne vrednosti adsorpcije CO_2 (9,69 mmol/g) na 27°C i 100 bara. PPAC se pojavljuje kao obećavajuće rešenje za hvatanje CO_2, nudeći vredne izglede za smanjenje emisija i rešavanje izazova klimatskih promena.

Ključne reči: *aktivni ugalj od kore zrele banane, metodologija površine odgovora, karakterizacija, optimizacija, adsorpcija CO_2*

Naučni rad
Rad primljen: 17.11.2023.
Rad prihvaćen: 10.12.2023.
Rad je dostupan na sajtu: www.idk.org.rs/casopis